Published in final edited form as:

Kidney Int. 2020 October ; 98(4): 958–969. doi:10.1016/j.kint.2020.05.027.

Novel nephronophthisis-associated variants reveal functional importance of MAPKBP1 dimerization for centriolar recruitment

Ria Schönauer[1], **Wenjun Jin**[1], **Anastasia Ertel**[1], **Melanie Nemitz-Kliemchen**[1], **Nydia Panitz**[1], **Elena Hantmann**[1], **Anna Seidel**[1], **Daniela A. Braun**[2], **Shirlee Shril**[2], **Matthias Hansen**[3], **Khurrum Shahzad**[4], **Richard Sandford**[5], **Sophie Saunier**[6], **Alexandre Benmerah**[6], **Carsten Bergmann**[7,8,9], **Friedhelm Hildebrandt**[2], **Jan Halbritter**[1]

[1]Division of Nephrology, University Hospital Leipzig Medical Center, Leipzig, Germany

[2]Department of Medicine, Division of Nephrology, Boston Children's Hospital, Harvard Medical School, Boston, Massachusetts, USA

[3]Kuratorium für Dialyse und Nierentransplantation e. V. Center of Pediatric Nephrology, Clementine Children's Hospital, Frankfurt, Germany

[4]Institute of Laboratory Medicine, Clinical Chemistry and Molecular Diagnostic, Leipzig, Germany

[5]Academic Department of Medical Genetics, University of Cambridge, Cambridge, UK

[6]Université de Paris, Imagine Institute, Laboratory of inherited kidney diseases, INSERM UMR 1163, Paris, France

[7]Center for Human Genetics, Bioscientia, Ingelheim, Germany

[8]Department of Medicine, University Hospital Freiburg, Freiburg, Germany

[9]Medizinische Genetik Mainz, Limbach Genetics, Mainz, Germany

Abstract

Biallelic mutations in *MAPKBP1* were recently associated with late-onset cilia-independent nephronophthisis. MAPKBP1 was found at mitotic spindle poles but could not be detected at primary cilia or centrosomes. Here, by identification and characterization of novel *MAPKBP1* variants, we aimed at further investigating its role in health and disease. Genetic analysis was done by exome sequencing, homozygosity mapping, and a targeted kidney gene panel while coimmunoprecipitation was used to explore wild-type and mutant protein-protein interactions. Expression of MAPKBP1 in non-ciliated HeLa and ciliated inner medullary collecting duct cells enabled colocalization studies by fluorescence microscopy. By next generation sequencing, we identified two novel homozygous *MAPKBP1* splice-site variants in patients with

Correspondence: Jan Halbritter, Department of Internal Medicine, Division of Nephrology, University Hospital Leipzig, Liebigstrasse 20, 04103 Leipzig, Germany. Jan.Halbritter@medizin.uni-leipzig.de.

AUTHOR CONTRIBUTIONS

RSc and JH designed the study. FH, SSa, and AB contributed to experimental conception. RSc, WJ, AE, MN-K, NP, EH, AS, and KS carried out experiments. RSc analyzed the data. RSc, DAB, SSh, CB, and FH conducted genetic analyses. RSa and MH contributed clinical data. RSc created the figures. RSc and JH drafted and revised the paper. All authors approved the final version of the manuscript.

DISCLOSURE

All the authors declared no competing interests.

nephronophthisis-related chronic kidney disease. Splice-site analyses revealed truncation of C-terminal coiled-coil domains and patient-derived deletion constructs lost their ability to homodimerize and heterodimerize with paralogous WDR62. While wild-type MAPKBP1 exhibited centrosomal, basal body, and microtubule association, mutant proteins lost the latter and showed reduced recruitment to cell cycle dependent centriolar structures. Wild-type and mutant proteins had no reciprocal influence upon co-expression excluding dominant negative effects. Thus, MAPKBP1 appears to be a novel microtubule-binding protein with cell cycle dependent centriolar localization. Truncation of its coiled-coil domain is enough to abrogate its dimerization and results in severely disturbed intracellular localizations. Delineating the impact of impaired dimerization on cell cycle regulation and intracellular kidney signaling may provide new insights into common mechanisms of kidney degeneration. Thus, due to milder clinical presentation, MAPKBP1-associated nephronophthisis should be considered in adult patients with otherwise unexplained chronic kidney disease.

Keywords

centrosome; chronic kidney disease; cilia; MAPKBP1; microtubules; nephronophthisis; scoliosis; tubulointerstitial nephritis; WDR62

Biallelic pathogenic variants within *MAPKBP1*, encoding mitogen-activated protein kinase binding protein 1, were recently reported to cause juvenile, late-onset, cilia-independent nephronophthisis ([NPH], Mendelian Inheritance in Man [MIM] #617271 [Online Mendelian Inheritance in Man, www.omim.org]).[1] NPH is an autosomal-recessive kidney disorder with common extrarenal organ involvement frequently accounting for end-stage renal disease (ESRD) in childhood and adolescence, and recent data underline that its prevalence is underestimated in adult-onset ESRD.[2] Renal degeneration in NPH is histologically characterized by chronic tubulointerstitial nephritis and renal fibrosis.[3] NPH is classified as ciliopathy, as the majority of the so far identified 20 disease-associated genes play key roles in primary cilia function of renal tubular epithelial cells. However, recently discovered NPH genes including *MAPKBP1* (also known as *NPHP20*), pointed to cilia-independent functions, including alterations of the DNA damage-response pathway.[1,4]

MAPKBP1 is a 170 kDa scaffolding protein[5] consisting of an N-terminal WD40 domain, a c-Jun N-terminal kinase (JNK)-binding domain, and a C-terminal dimerization domain. However, its physiological role largely remains unknown and only a small number of studies focused on detailed functional aspects.[5–8] However, its JNK-binding paralog WDR62, a microcephaly-associated protein (MIM# 604317),[9] was intensively studied and found to be recruited to specialized granular cell compartments upon stress induction together with MAPKBP1.[7,10] MAPKBP1 was speculated to play a role in cell cycle regulation, as mutant variants unlike the wild type (WT) were not able to colocalize with WDR62 at mitotic spindle poles (MSPs).[1] Because virtually all initially reported NPH-associated *MAPKBP1* variants led to a premature stop codon resulting in loss of its C-terminal dimerization domain, abrogation of interaction between the 2 paralogs WDR62 and MAPKBP1 was proposed as a potential mechanism of disease.[1] However, as WDR62 deficiency does not result in kidney disease in mice and humans,[9,11] alternative mechanisms of MAPKBP1-

associated NPH, independent from abrogated WDR62 interaction, remain to be elucidated. In this study, identification of 2 additional disease-associated *MAPKBP1* variants prompted us to gain deeper insights into its physiological function to unravel novel mechanisms of renal degeneration and fibrosis.

RESULTS

Identification of novel *MAPKBP1* splice-site variants associated with NPH

First, by means of exome sequencing, we identified a novel homozygous splice-site variant (c.4317+5G>C) in a 37-year-old Caucasian female (patient 1), born from first-degree cousins. She first presented with cystic, nonenlarged, fibrotic kidneys in adolescence (Table 1, Figure 1b). Kidney disease was clinically diagnosed as NPH and resulted in ESRD at age 23, which was treated by subsequent renal transplantation. Additionally, the patient displayed a Marfanoid habitus with arachnodactyly, scoliosis, and facial dysmorphism, but normal intellectual development. As the most prominent extrarenal disease manifestation, she showed massive scoliosis requiring surgical stabilization by Harrington rods (Table 1, Figure 1b). Extrarenal disease was clinically diagnosed as Ehlers-Danlos syndrome kyphoscoliotic type 1 (MIM# 225400), however, without identification of an underlying genetic diagnosis by analysis of known Ehlers-Danlos syndrome genes.

Second, targeted next-generation sequencing-based renal gene panel analysis for clinically suspected NPH yielded a novel homozygous splice site variant (c.3333-2A>G) in a 14-year-old female from healthy parents of Syrian origin (patient 2) (Table 1, Figure 1c). Clinically, patient 2 presented with increased renal echogenicity, solitary bilateral kidney cysts, and chronically impaired glomerular filtration rate (chronic kidney disease [CKD] stage G3b). Additionally, patient 2 displayed growth retardation and a vascular anomaly of the inferior vena cava, with partial malrotation to the left, merging into the left renal vein. In accordance with a recessive disorder, all parents were clinically unaffected and segregation analysis of patient 1 by Sanger sequencing revealed maternal and paternal heterozygosity (Figure 1b and c: i, ii).

Alternative splicing produces 2 aberrant transcripts with premature stop

As both identified variants locate to splice sites close to the 3′ end of *MAPKBP1*, we sought to analyze aberrant splicing on the RNA level (Figure 1a). RNA extraction, cDNA synthesis, and Sanger sequencing of patient blood samples allowed for investigation of the splicing impact. Variant c.4317+5G>C at splice-donor site of intron 31 leads to integration of 138 intronic base pairs, resulting in a premature stop codon within the retained intron (p.Gly1442Valfs*12) (Figure 1b; Supplementary Data S1A). In contrast, cDNA analysis of c.3333-2A>G at splice-acceptor site of intron 28, revealed 3 different transcripts resulting from the integration of intronic sequences of varying lengths (Figure 1c; Supplementary Data S1B). Full (261 base pairs) or partial (87 or 51 base pairs) intron retention leads to different premature stop codons resulting in 3 distinct truncated proteins (p.Glu1112Tyrfs*41, p.Arg1111Serfs*5, and p.Pro1113Glufs*2). Thus, alternative splicing yields formation of aberrant MAPKBP1 proteins truncated within the putative C-terminal CC (patient 1) or JNK binding domain (patient 2) (Figure 2a).

Loss of homo- and heterodimerization ability in patient-derived deletion constructs

To investigate the impact of identified novel truncated MAPKBP1 proteins on a functional level, expression plasmids with N-terminal green fluorescent protein (GFP) or red fluorescent protein (RFP) fusion proteins and C-terminal DDK- or hemagglutinin (HA)-tags were constructed (Figure 2a). For patient 1, additional intronic amino acids including the premature stop codon were introduced to generate the plasmid G1442Vfs*12, whereas the artificial truncating protein construct E1112* was prepared as surrogate to investigate functional consequences of the differential protein products of patient 2.

Recapitulating previous reports on WDR62, *in silico* modeling of MAPKBP1 tertiary structure indicated the last 200 amino acids to form 3 α-helices comprising CC domain (Figure 2b and c).[7] Coimmunoprecipitation using HEK293 cells transiently cotransfected with HA-tagged WDR62 WT and DDK-tagged MAPKBP1 variants demonstrated abrogation of interaction of truncated MAPKBP1 proteins with WDR62 (Figure 2d). Because previous investigations demonstrated homodimerization of short C-terminal MAPKBP1 constructs,[7] we investigated the interaction of full-length HA-tagged MAPKBP1 with WT and mutant DDK-tagged MAPKBP1. Interestingly, coimmunoprecipitation also showed loss of binding capacity for both truncated variants in contrast to proper homodimerization of WT proteins (Figure 2d).

MAPKBP1 localizes to centrosomes unlike patient-derived deletion constructs

Recent studies reported MAPKBP1 to neither localize to primary cilia nor centrosomes.[1] Instead it was present at MSPs during early phases of mitosis together with WDR62, which was absent for patient-derived proteins.[1] Therefore, GFP- and RFP-tagged MAPKBP1 plasmids (Figure 2a) were transiently transfected in HeLa cells to investigate the intracellular localization in nonciliated human cells in absence of mitosis.

Surprisingly, GFP-MAPKBP1 WT was found to localize to the centrosome in nondividing cells, demonstrated by colocalization with PCNT (Figure 3a: i-vi). In a subset of cells, MAPKBP1 was additionally observed in a filamentous pattern emerging from the centrosomal region (Figure 3a: iv). Furthermore, the majority of cells contained additional granular MAPKBP1 structures. While centrosomal localization was observed in all cells expressing WT MAPKBP1, in some cells a punctate pattern clustered around the centrosomal region (Figure 3a: v) and in others granules distributed throughout the cytoplasm (Figure 3a: vi). In contrast, both patient variants (G1442Vfs*12 and E1112*) diffusely localized to the cytosol (Figure 3a: vii and x) and nucleus (Figure 3a: viii and xi). Specificity of MAPKBP1 signals was validated by additional staining of C-terminal DDK-tags to exclude accumulation of cleaved GFP (Supplementary Figure S1). A granular/punctate distribution pattern was only occasionally observed for truncated variants, which instead localized at midbodies, unlike the WT (Figure 3a: ix and xii). Quantification of intracellular localization patterns revealed a predominantly noncytosolic distribution for WT in contrast to patient cells (Figure 3b). Whereas WT MAPKBP1 was localized to the centrosome in 80% of transfected cells, centrosomal recruitment of truncated variants was only observed in 10% of cases. Furthermore, intensity measurements revealed a 3-fold

reduced centrosomal accumulation of patient variants compared with the WT, whereas cytosolic intensity was 2-fold increased (Figure 3c).

MAPKBP1 WT associates with centrioles and microtubules

A deeper investigation of the centrosomal localization of MAPKBP1 WT revealed a specific pattern suggestive for a differential recruitment to mother and daughter centrioles (Figure 4a and b). Whereas daughters presumably possessed only a single accumulation, mothers appeared decorated with 3 separate MAPKBP1 speckles that also presented as ring structure depending on the orientation of the mother centriole relative to the focal plane (Figure 4b).

We next sought to characterize the nature of filamentous distribution of WT MAPKBP1. Because WDR62 was previously shown to be associated with the microtubule network, we stained HeLa cells transiently transfected with GFP constructs using an α-TUB antibody (Figure 4c). Filamentous structures observed in MAPKBP1 WT cells consistently colocalized with microtubules. Conversely, both patient variants (G1442Vfs*12 / E1112*) exhibited no visible filamentous distribution or pronounced colocalization with microtubules (Figure 4c). In some instances, MAPKBP1 WT granules were also found to localize along microtubule strands.

To also characterize the nature of MAPKBP1 granular structures, we performed coexpression with selected marker proteins. Earlier studies reported on granule formation of MAPKBP1 and WDR62 colocalizing at DCP1A-positive processing bodies (PBs) [7,10]; structures that have already been shown to associate with microtubules. HeLa cells were transiently cotransfected with fluorescently tagged WT MAPKBP1 and markers of stress granules (SGs) (GFP-G3BP, RFP-TIA1) or PBs (RFP-DCP1A) (Supplementary Figure S2). However, none of the investigated marker proteins colocalized with observed MAPKBP1 granules in absence of additional stress induction by arsenite, heat, cold, or ultraviolet irradiation (Supplementary Figure S2).

Nonrescue and absence of dominant-negative effects by WT-mutant coexpression

To further characterize the impact of impaired homodimerization on intracellular MAPKBP1 localization, we cotransfected HeLa cells with equal amounts of RFP-tagged MAPKBP1 WT and different GFP-tagged variants (Figure 5). RFP- and GFP-tagged WT combinations showed colocalization for all previously described localization patterns, including centrosomal, filamentous, and granular distributions. However, coexpression of MAPKBP1 WT had no major impact on disturbed intracellular distribution of patient variants, which were still found to be diffusely distributed in the cytosol and nucleus. Conversely, the presence of truncated MAPKBP1 variants had no influence on adequate intracellular distribution of MAPKBP1 WT.

MAPKBP1 localizes to centrosomes and basal bodies in ciliated cells unlike patient-derived deletion constructs

To analyze MAPKBP1 localization in a ciliated kidney cell system, we employed murine inner medullary collecting duct cells for overexpression of aforementioned human WT and mutant constructs (Figure 6, Supplementary Figure S3). In line with the previous report,[1]

gross primary cilia morphology, labeled with anti-acetylated α-TUB, was unchanged on overexpression of patient-derived deletion constructs. Interestingly, in addition to centrosomal localization, we observed MAPKBP1 WT protein at the ciliary base, compatible with basal body localization in quiescent cells. Analogous to diminished centrosomal expression of mutant MAPKBP1 in nonciliated HeLa cells, recruitment to centrosomes and basal bodies was markedly reduced or even absent in the case of C-terminal deletion (G1442Vfs*12 and E1112*) (Figure 6; Supplementary Figure S3).

DISCUSSION

By identification of 2 novel homozygous *MAPKBP1* splice-site variants associated with NPH and CKD, we extend functional insights into MAPKBP1 function in health and disease. Patients with MAPKBP1 defects present with non-congenital, adolescent (patient 2) or even adult NPH (patient 1), and seem overall less severely affected than in many other NPH-associated ciliopathies.[12] Only 2 of 10 published cases to date exhibited ESRD before adulthood, at 12 and 15 years, respectively.[1] This observation has implications for clinicians to be aware of NPH also in adult-onset CKD patients, notably in those with oligo- or microcystic atrophic kidneys and undetermined chronic tubulointerstitial nephritis, which may indicate NPH on renal histology. In contrast to autosomal-dominant tubulointerstitial kidney disease,[13] parents are expected to be unaffected and family history is often negative. Recently, homozygous *NPHP1* deletions, the most frequent genetic NPH-associated alteration, were found to account for 0.5% of adult-onset ESRD in a large population screening.[2] Similarly, pathogenic *MAPKBP1* variants have to be considered in young adults with otherwise unexplained ESRD, a phenomenon that was shown to pertain to 20% to 40% of the patients on renal replacement therapy waiting for kidney transplantation.[14,15] Detection of pathogenic *MAPKBP1* variants should prompt screening for skeletal abnormalities, as those were present in 8 of 10 reported cases to date.[1] Notably scoliosis (as in patient 1) was already observed previously in 3 affected family members with an adjacent homozygous truncating mutation (p.Gln943*).[1] Collectively, scoliosis, long fingers (patient 1 plus individual already reported in previous report), and vascular anomalies (patient 2) appear somewhat reminiscent of connective tissue disorders, such as Ehlers-Danlos syndrome and patient 1 was even clinically diagnosed as such (kyphoscoliotic, type 1), however, without genetic confirmation. Therefore, it is well conceivable that these clinical signs represent extrarenal manifestations of defective MAPKBP1. Remarkably, identified patients almost exclusively harbored truncating variants, suggesting a major mechanistic role of disturbed C-terminal binding capacity in renal degeneration.[1] In addition to abrogated heterodimerization of MAPKBP1 with WDR62, we were able to show impaired homodimerization ability of MAPKBP1 for newly identified patient variants.[7]

While previous studies detected MAPKBP1 at MSPs and stress granules on stress induction,[1,7] here we demonstrate that WT MAPKBP1 is a microtubule-binding protein with cell cycle–dependent recruitment to centrosomes, basal bodies, and MSPs in ciliated and nonciliated cell systems. Inversely, truncated patient variants lost their microtubule binding capacity and showed severely disturbed intracellular distribution with predominant cytosolic and nuclear localization at the expense of centriolar recruitment. The differences in MAPKBP1 localization to previous studies might be explained by very low expression of

endogenous MAPKBP1 under nonstressed conditions and an increased signal intensity and specificity obtained with fluorescent proteins compared with the low signal-to-background ratios in antibody-treated cells, because centrosomal accumulation could hardly be detected by staining of the C-terminal DDK-tag. More detailed, in HeLa cells, we found that mother centrioles appeared to be decorated with major MAPKBP1 WT accumulations in a 3-dotted pattern or ring structure, whereas daughter centrioles only comprised smaller amounts concentrated at a single location. Similar patterns were already described for other centrosomal proteins located at the subdistal appendages of the mother centriole that anchor cytoplasmic microtubules and the proximal ends of both centrioles, including ninein, CEP110, CEP170, KIF2A, and the p150glued/dynactin complex.[16,17] Subdistal appendage localization was reported for other NPH-related proteins such as CC2D2A playing a major role in subdistal appendage assembly and axonemal establishment[18] and SDCCAG8[19] being implicated in DNA damage pathways similar to MAPKBP1.[12] Moreover, WDR62 was recently found to be involved in ciliogenesis,[20] centriole biogenesis, regulation of apical complex, and cell fate by interaction with the proximal ends of mother centrioles in neural progenitors, thereby underlining the existence of shared mechanisms but specialized functions for WDR62 and MAPKBP1.[21]

As overexpression of WT *MAPKBP1* in HeLa cells exhibited a marked filamentous distribution in addition to centrosomal localization, we suspected MAPKBP1 to bind to the microtubule network. Indeed, the WT was found to colocalize with α-TUB and, moreover, MAPKBP1 granules appeared to be distributed along the microtubule filaments. Similar to centrosomal localization, patient variants mainly lost their microtubular association. Because truncated variants were not able to form granules, we assume that the C-terminal domain is required for their generation and enhances localization to microtubules. In contrast, interaction of WDR62 with microtubules was shown to depend on the N-terminal WD40 domain,[22] which was still present in our investigated MAPKBP1 variants. However, microtubule and spindle pole association of WDR62 is differentially regulated by interaction with *AURKA* kinase and JNK, and binding of the latter was shown to be influenced by dimerization of WDR62.[7,22] Thus, we speculate that the WD40 domain of MAPKBP1 is necessary for centrosomal or microtubular association, but efficient targeting to these structures probably involves additional mechanisms that require the CC domain.

Unexpectedly, besides cytosolic and nuclear distribution, investigation of the truncated MAPKBP1 patient variants additionally revealed a strong accumulation at the midbody of dividing cells or its remnant. Recent studies reported a common set of proteins to be localized to the midbody, basal body, or primary cilia,[23] including intraflagellar transport complex proteins and p150glued,[24,25] and revealed a role for midbody remnants in the initiation of primary cilia assembly.[26] Because neither nuclear nor midbody localization was detectable for the WT, we assume mistargeting to these structures depending on dysregulated interaction with other proteins arising from the lack of the C-terminus. Lastly, we could not find any noticeable mutual influence on the localization patterns of MAPKBP1 WT and patient variants on cotransfection, which is in agreement with the heterozygous state not being sufficient to induce NPH phenotypes.

In summary, we extend the genotypic and phenotypic spectrum of MAPKBP1-associated NPH and provide additional information on its intracellular localization and function. For the first time, we characterize MAPKBP1 as a microtubule-binding protein and demonstrate its cell cycle–dependent localization to centrosomes in nonciliated and basal bodies in ciliated cells by a distinct centriolar pattern (Figure 7). All of these localizations were diminished or abrogated for C-terminally truncated patient-derived proteins lacking the C-terminal CC domain that instead were diffusely mistargeted to cytosol, nucleus, and midbody of dividing cells. Thus, these aberrant intracellular localizations of MAPKBP1 provide a plethora of potential mechanistic links, including regulation of the microtubular network, the MSP, cell division, cell cycle checkpoints, as well as ciliary and nonciliary cargo transport potentially contributing to renal degeneration. Further studies have to investigate the functional interplay between centrosomopathies and ciliopathies to unravel interconnections between cilia-dependent and independent functions of NPH-related proteins. Identification of the underlying molecular mechanism in rare kidney disorders such as NPH may also serve as a model for understanding and subsequent targeting of disease mechanisms of common renal degeneration in the growing number of CKD patients.

METHODS

Sequencing

To identify additional genes mutated in NPH, we independently performed homozygosity mapping, exome sequencing, and targeted next-generation sequencing multigene panel testing on affected individuals. In brief, we used a customized sequence capture library, as previously described[27] (see detailed methods in Supplementary Data S1). Written informed consent was obtained from all individuals enrolled in this study and approved by the Institutional Review Board at the Boston Children's Hospital and the University of Leipzig. For splice-site analysis, RNA was extracted from patient blood samples and transcribed into cDNA. Regions of interest were amplified with custom-designed primers and subjected to Sanger sequencing (Core Unit DNA-Technologies, Leipzig University, Leipzig, Germany).

In silico structure prediction

Structure of the C-terminal CC domain was generated using the QUARK server (Quark, New York, NY).[13,14]

Expression vectors

MAPKBP1 and WDR62 plasmids pcDNA3.1D_JNKBP1/V5-6xHis-TOPO and pCAN3_WDR62 were previously published.[1] For WDR62, N-terminal myc-was replaced by HA- and for MAPKBP1 C-terminal V5- by 2xDDK- or HA-tag sequences using the Q5 Site-Directed Mutagenesis Kit (New England Biolabs, Ipswich, MA). For G1442Vfs*12, intronic bases were introduced, whereas E1112* was constructed by introduction of a stop codon at amino acid position 1112 (Supplementary Data S2). For N-terminal GFP-tags the GFP-sequence of TagGFP2-hPC2 (P. Harris and V. E. Torres, Mayo Clinic, Rochester, MN) was amplified with primers containing HindIII restriction sites. Polymerase chain reaction products and plasmids were ligated with T4 DNA Ligase after digestion (Thermo Fisher Scientific, Waltham, MA). To generate N-terminally RFP-tagged MAPKBP1, pCMV6-AN-

mRFP (OriGene Technologies, Rockville, MD) and pcDNA3.1D_JNKBP1/2xDDK-His-TOPO were digested with FastDigest MssI and FastDigest HindIII (FD1344; Thermo Fisher Scientific). Site-directed mutagenesis polymerase chain reaction was performed to restore the correct reading frame. Sequences were verified by Sanger sequencing. Plasmids encoding p-EGFP-G3BP+STOP, mRFP-Dcp1a, and mRFP-TIA1 were kindly provided by N. Kedersha (Brigham and Woman's Hospital, Boston, MA).[28]

Antibodies

Detailed information about antibodies is provided in Supplementary Data S3.

Immunoprecipitation and Western blotting

HEK293 (DSMZ, Braunschweig, Germany) were grown to 60% to 80% confluence in T25 cell culture flasks with Dulbecco's Modified Eagle's Medium/Ham's F12 (DMEM/F12) (Gibco, Thermo Fisher Scientific) with 15% FBS Superior (Biochrom, Merck Millipore, Merck, Darmstadt, Germany) under humidified atmosphere at 37 °C and 5% CO_2. Transfection was performed for 24 hours with 1 µl Lipofectamine 3000 and 2 µl P3000^T Enhancer Reagent per 1 µg plasmid in Opti-MEM (Gibco, Thermo Fisher Scientific)/ DMEM/ F12 (1/1.5/1.5) + 15% fetal bovine serum (FBS). Cells were lysed in Pierce RIPA buffer or Pierce IP Lysis Buffer supplemented with Halt Protease and Phosphatase Inhibitor Cocktail (100×) to prepare lysate and samples for immunoprecipitation using the Pierce HA-Tag Magnetic IP/Co-IP Kit. Samples were prepared with NuPAGE LDS Sample Buffer (4×) and SDS-gel runs, and Western blotting was performed with an iBlot 2 System using NuPAGE 3% to 8% Tris-Acetate Protein Gels, NuPAGE Tris-Acetate SDS Running Buffer (20×), and iBlot 2 Transfer Stacks (PVDF). All reagents were purchased from Thermo Fisher Scientific.

Immunofluorescence microscopy

HeLa (ATCC, Manassas, VA) and IMCD cells (Bernhard Schermer, University Hospital Cologne, CECAD Research Center) were grown to 60% to 80% confluence on µ-Slide 8 Wells (ibidi, Martinsried, Germany) in DMEM (Gibco, Thermo Fisher Scientific) with 10% FBS or DMEM/F12 with 15% FBS, respectively, under humidified atmosphere at 37 °C and 5% CO_2. HeLa and IMCD cells were transfected for 3 hours with 1 µl Lipofectamine 2000 and 3000 (Invitrogen, Thermo Fisher Scientific), respectively, per 1 µg plasmid in Opti-MEM/DMEM/F12 (1/1.5/1.5) without FBS and incubated in fresh DMEM + FBS overnight. For antibody staining, cells were fixed, permeabilized, and blocked using the Image-iT Fixation/Permeabilization Kit (Invitrogen, Thermo Fisher Scientific) or Permeabilization Solution (Sigma-Aldrich/Merck, Darmstadt, Germany). Antibodies (Supplementary Data S3) were incubated for 1 to 3 hours as phosphate-buffered saline dilutions (Thermo Fisher Scientific) at room temperature. Nuclei were stained for 10 minutes with NucBlue Fixed Cell ReadyProbes Reagent (Invitrogen, Thermo Fisher Scientific) and cells were sealed with ibidi Mounting Medium. Slides were documented using an AxioObserver.Z1 microscope with an ApoTome Imagig System and analyzed with the ZEN light software (Carl Zeiss AG, Oberkochen, Germany). Localization of MAPKBP1 variants in HeLa cells was compared for ≥100 fixed cells per condition of 3 independent transfections, quantification of centrosomal intensity was based on ≥50 and ≥30 cells of at least 2 and 3 independent

transfections for HeLa and IMCD cells, respectively. Statistical analysis and intensity measurements were performed with the GraphPad Prism 5 software (GraphPad Software, La Jolla, California) using regular 2-way ANOVA with Turkey correction and 95% confidence intervals.

Supplementary Material

Refer to Web version on PubMed Central for supplementary material.

ACKNOWLEDGMENTS

We thank all patients and their families for participating in this study. Nancy Kedersha, Peter Harris, and Vicente E. Torres are kindly acknowledged for providing expression plasmids encoding fluorescently labeled proteins. RSc has received support by an intramural young investigator funding from the University of Leipzig. The University of Cambridge has received salary support in respect to RSa from the National Health Service in the East of England through the Clinical Academic Reserve. KS receives funding from Deutsche Forschungsgemeinschaft (grant SH 849/1-2) and of the Stiftung Pathobiochemie und Molekulare Diagnostik. CB was an employee of Bioscientia/Sonic Healthcare until September 2019. Since then he has been an employee of the Limbach group and heads and manages Limbach Genetics. His research laboratory at the University of Freiburg receives support from the Deutsche Forschungsgemeinschaft (BE 3910/8-1, BE 3910/9-1, and project no. 246781735—Collaborative Research Centre KIDGEM 1140) and the Federal Ministry of Education and Research (01GM1903I and 01GM1903G). FH was supported by a grant from the National Institutes of Health (R01-DK068306). JH receives funding from Deutsche Forschungsgemeinschaft (HA 6908/2-1), Else Kroner-Fresenius Stiftung (2016_A52), Fritz Thyssen Foundation, and Integriertes Forschungs- und Behandlungszentrum–Federal Ministry of Education and Research. This work was supported by the Federal Ministry of Education and Research (FKZ 01EO1501).

REFERENCES

1. Macia MS, Halbritter J, Delous M, et al. Mutations in MAPKBP1 cause juvenile or late-onset cilia-independent nephronophthisis. Am J Hum Genet. 2017;100:323–333. [PubMed: 28089251]
2. Snoek R, van Setten J, Keating BJ, et al. NPHP1 (nephrocystin-1) gene deletions cause adult-onset ESRD. J Am Soc Nephrol. 2018;29:1772–1779. [PubMed: 29654215]
3. Stokman M, Lilien M, Knoers N. GeneReviews®: Nephronophthisis. Seattle, WA: University of Washington, Seattle; 1993.
4. Chaki M, Airik R, Ghosh AK, et al. Exome capture reveals ZNF423 and CEP164 mutations, linking renal ciliopathies to DNA damage response signaling. Cell. 2012;150:533–548. [PubMed: 22863007]
5. Koyano S, Ito M, Takamatsu N, et al. A novel Jun N-terminal kinase (JNK)-binding protein that enhances the activation of JNK by MEK kinase 1 and TGF-beta-activated kinase 1. FEBS Lett. 1999;457:385–388. [PubMed: 10471813]
6. Lecat A, Di Valentin E, Somja J, et al. The c-Jun N-terminal kinase (JNK)-binding protein (JNKBP1) acts as a negative regulator of NOD2 protein signaling by inhibiting its oligomerization process. J Biol Chem. 2012;287:29213–29226. [PubMed: 22700971]
7. Cohen-Katsenelson K, Wasserman T, Darlyuk-Saadon I, et al. Identification and analysis of a novel dimerization domain shared by various members of c-Jun N-terminal kinase (JNK) scaffold proteins. J Biol Chem. 2013;288:7294–7304. [PubMed: 23341463]
8. Yamaguchi T, Miyashita C, Koyano S, et al. JNK-binding protein 1 regulates NF-kappaB activation through TRAF2 and TAK1. Cell Biol Int. 2009;33:364–368. [PubMed: 19385034]
9. Bilgüvar K, Oztürk AK, Louvi A, et al. Whole-exome sequencing identifies recessive WDR62 mutations in severe brain malformations. Nature. 2010;467:207–210. [PubMed: 20729831]
10. Wasserman T, Katsenelson K, Daniliuc S, et al. A novel c-Jun N-terminal kinase (JNK)-binding protein WDR62 is recruited to stress granules and mediates a nonclassical JNK activation. Mol Biol Cell. 2010;21:117–130. [PubMed: 19910486]

11. Sgourdou P, Mishra-Gorur K, Saotome I, et al. Disruptions in asymmetric centrosome inheritance and WDR62-Aurora kinase B interactions in primary microcephaly. Sci Rep. 2017;7:43708. [PubMed: 28272472]
12. Srivastava S, Molinari E, Raman S, Sayer JA. Many genes-one disease? Genetics of nephronophthisis (NPHP) and NPHP-associated disorders. Front Pediatr. 2018;5:287. [PubMed: 29379777]
13. Eckardt K-U, Alper SL, Antignac C, et al. Autosomal dominant tubulointerstitial kidney disease: diagnosis, classification, and management—a KDIGO consensus report. Kidney Int. 2015;88:676–683. [PubMed: 25738250]
14. Kramer A, Pippias M, Noordzij M, et al. The European Renal Association—European Dialysis and Transplant Association (ERA-EDTA) Registry Annual Report 2015: a summary. Clin Kidney J. 2018;11:108–122. [PubMed: 29423210]
15. Ottlewski I, Münch J, Wagner T, et al. Value of renal gene panel diagnostics in adults waiting for kidney transplantation due to undetermined end-stage renal disease. Kidney Int. 2019;96:222–230. [PubMed: 31027891]
16. Ou YY, Mack GJ, Zhang M, Rattner JB. CEP110 and ninein are located in a specific domain of the centrosome associated with centrosome maturation. J Cell Sci. 2002;115:1825–1835. [PubMed: 11956314]
17. Mazo G, Soplop N, Wang W-J, et al. Spatial control of primary ciliogenesis by subdistal appendages alters sensation-associated properties of cilia. Dev Cell. 2016;39:424–437. [PubMed: 27818179]
18. Veleri S, Manjunath SH, Fariss RN, et al. Ciliopathy-associated gene Cc2d2a promotes assembly of subdistal appendages on the mother centriole during cilia biogenesis. Nat Commun. 2014;5:4207. [PubMed: 24947469]
19. Vertii A, Bright A, Delaval B, et al. New frontiers: discovering ciliaindependent functions of cilia proteins. EMBO Rep. 2015;16:1275–1287. [PubMed: 26358956]
20. Shohayeb B, Ho U, Yeap YY, et al. The association of microcephaly protein WDR62 with CPAP/IFT88 is required for cilia formation and neocortical development. Hum Mol Genet. 2020;29:248–263. [PubMed: 31816041]
21. Jayaraman D, Kodani A, Gonzalez DM, et al. Microcephaly proteins Wdr62 and Aspm define a mother centriole complex regulating centriole biogenesis, apical complex, and cell fate. Neuron. 2016;92:813–828. [PubMed: 27974163]
22. Lim NR, Yeap YYC, Zhao TT, et al. Opposing roles for JNK and Aurora A in regulating the association of WDR62 with spindle microtubules. J Cell Sci. 2015;128:527–540. [PubMed: 25501809]
23. Otto EA, Hurd TW, Airik R, et al. Candidate exome capture identifies mutation of SDCCAG8 as the cause of a retinal-renal ciliopathy. Nat Genet. 2010;42:840–850. [PubMed: 20835237]
24. Taulet N, Vitre B, Anguille C, et al. IFT proteins spatially control the geometry of cleavage furrow ingression and lumen positioning. Nat Commun. 2017;8:1928. [PubMed: 29203870]
25. Kaplan A, Reiner O. Linking cytoplasmic dynein and transport of Rab8 vesicles to the midbody during cytokinesis by the doublecortin domaincontaining 5 protein. J Cell Sci. 2011;124:3989–4000. [PubMed: 22159412]
26. Bernabé-Rubio M, Alonso MA. Routes and machinery of primary cilium biogenesis. Cell Mol Life Sci. 2017;74:4077–4095. [PubMed: 28624967]
27. Lu H, Galeano MCR, Ott E, et al. Mutations in DZIP1L, which encodes aciliary-transition-zone protein, cause autosomal recessive polycystic kidney disease. Nat Genet. 2017;49:1025–1034. [PubMed: 28530676]
28. Kedersha N, Stoecklin G, Ayodele M, et al. Stress granules and processing bodies are dynamically linked sites of mRNP remodeling. J Cell Biol. 2005;169:871–884. [PubMed: 15967811]

Translational Statement

MAPKBP1 loss-of-function leads to nephronophthisis with premature renal degeneration, skeletal abnormalities, and chronic kidney disease (CKD). By identification of novel biallelic truncating variants, we reveal MAPKBP1 as a microtubule-binding protein with cell cycle–dependent localization to mitotic spindle poles, centrosomes, and basal bodies. Recruitment to these organelles requires dimerization via its C-terminal coiled-coil domain, which was lost in affected patients. Further understanding of MAPKBP1's function during the cell cycle may provide leverage for mitigating renal degeneration and CKD progression in nephronophthisis and beyond. Genetic analysis of *MAPKBP1* should be considered in young adults with undetermined chronic tubulointerstitial nephritis and unexplained CKD.

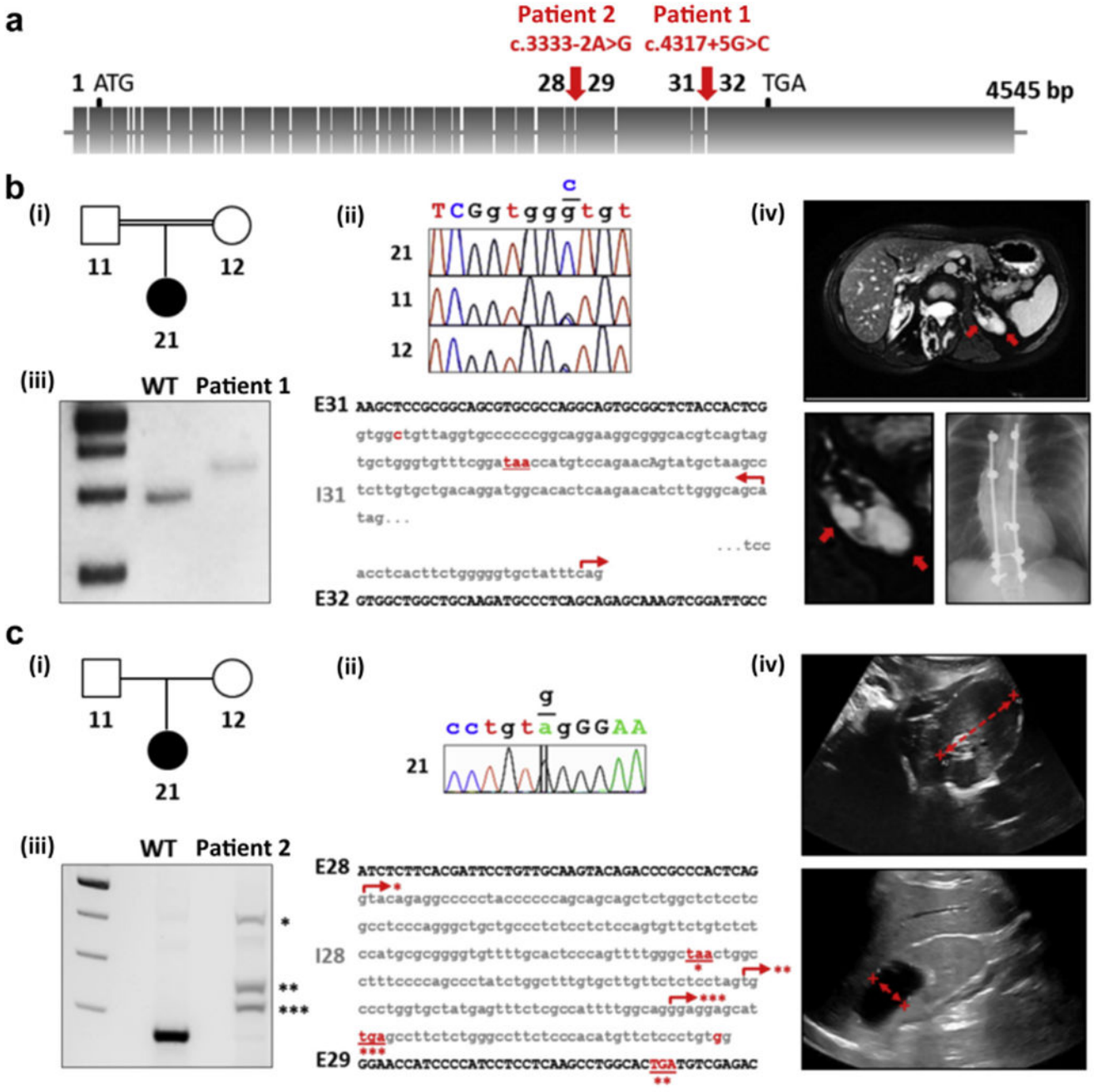

Figure 1 |. Genetic and clinical characterization of patients with novel nephronophthisis-associated *MAPKBP1* splice-site variants.

(**a**) Exon (E) structure of *MAPKBP1*: red arrows indicate splice-site variants located in the splice-acceptor site of intron (I) 31 (c.4317+5G>C, patient 1) and splice-donor site of intron 28 (c.3333-2A>G, patient 2) (start codon: ATG; stop codon: TGA). (**b**) Investigation of *MAPKBP1* c.4317+5G>C: (*i*) pedigree; (*ii*) chromatograms and segregation; (*iii*) agarose gel analysis of resulting cDNA transcript; sequencing revealed a retained intronic sequence (direction indicated by red arrows) and premature stop codon (red underlined letters); (*iv*) magnetic resonance imaging showing nonenlarged cystic kidneys (red arrows) and X-ray

displaying severe scoliosis stabilized by Harrington rods. (**c**) Investigation of *MAPKBP1* c.3333-2A>G: (*i*) pedigree; (*ii*) chromatogram; (*iii*) agarose gel analysis showing 3 distinct cDNA transcripts (marked by asterisks); sequencing revealed retained intronic sequences of different lengths (direction indicated by red arrows) resulting in different premature stop codons (red underlined letters); (*iv*) renal ultrasound showing hyperechogenic kidneys with solitary cysts. Uppercase black letters are exonic sequences; lowercase gray letters are intronic sequences; and red letters are the splice-site variant. bp, base pairs; WT, wild type.

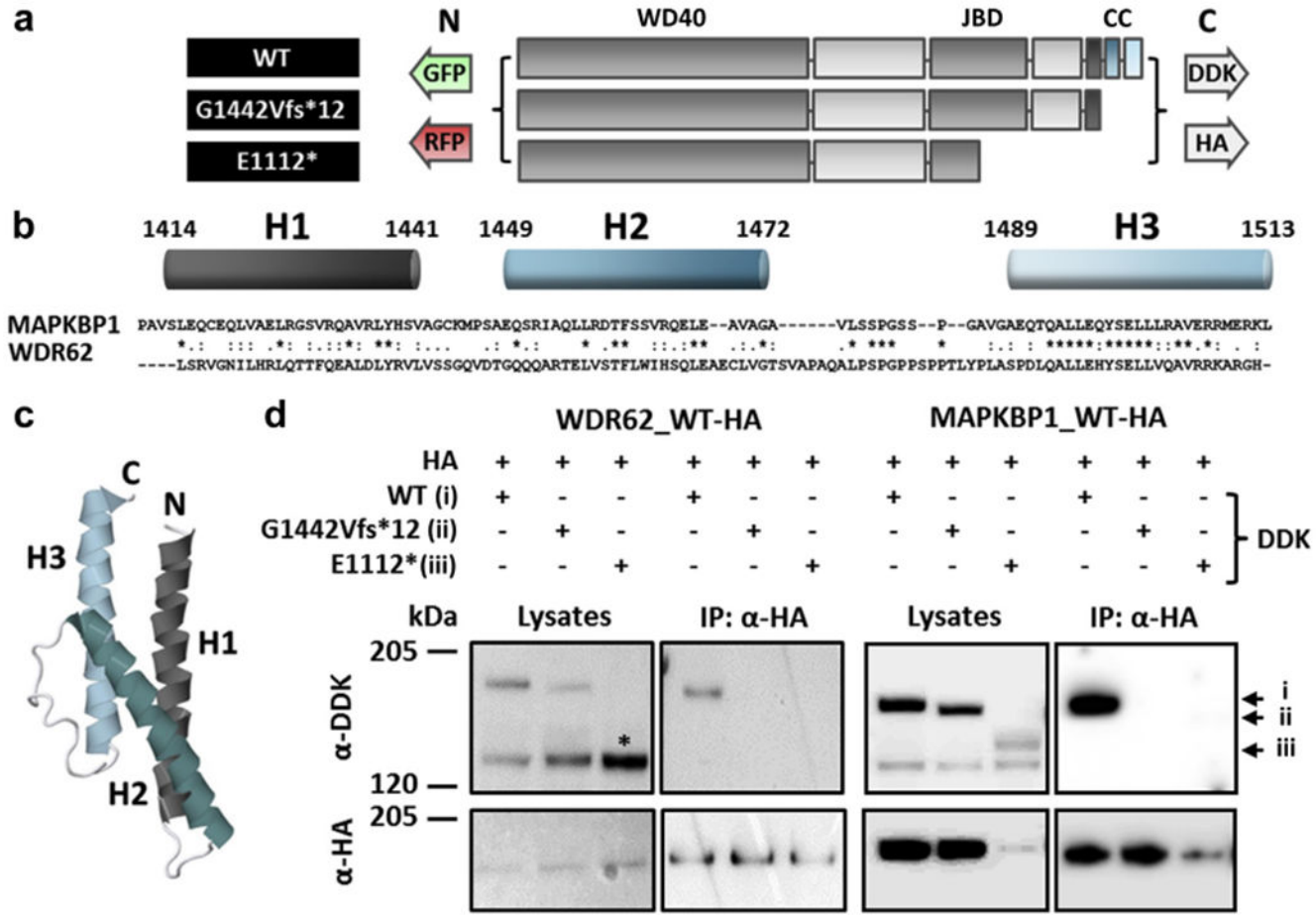

Figure 2 |. Coiled-coil (CC) domain mediates homo- and heterodimerization of MAPKBP1.

(**a**) Schematic representation of MAPKBP1 expression plasmids encoding wild-type (WT) and truncated patient-derived cDNA sequences (c.4317+5G>C, patient 1: G1442Vfs*12; c.3333-2A>G, patient 2: E1112*) with N-terminal (N) green fluorescent protein (GFP) or red fluorescent protein (RFP) fusion and C-terminal (C) DDK- or hemagglutinin (HA)-tags. (**b**) Alignment of the C-terminal 200 amino acids of MAPKBP1 with WDR62 including predicted α-helical regions (H1–H3). (**c**) *In silico* model of the MAPKBP1 C-terminal CC domain consisting of 3 α-helices (H1–H3) (QUARK[13]). (**d**) Coimmunoprecipitation of HA-tagged MAPKBP1 or WDR62 WT proteins with DDK-tagged MAPKBP1 variants. Asterisk denotes merging of truncated MAPKBP1-band (*iii*) with unspecific protein band. Homo- and heterodimerization of MAPKBP1 WT proteins is abrogated in C-terminally truncated variants. IP, immunoprecipitation; JBD, JNK-binding domain; WD40, WD40 repeat-containing domain.

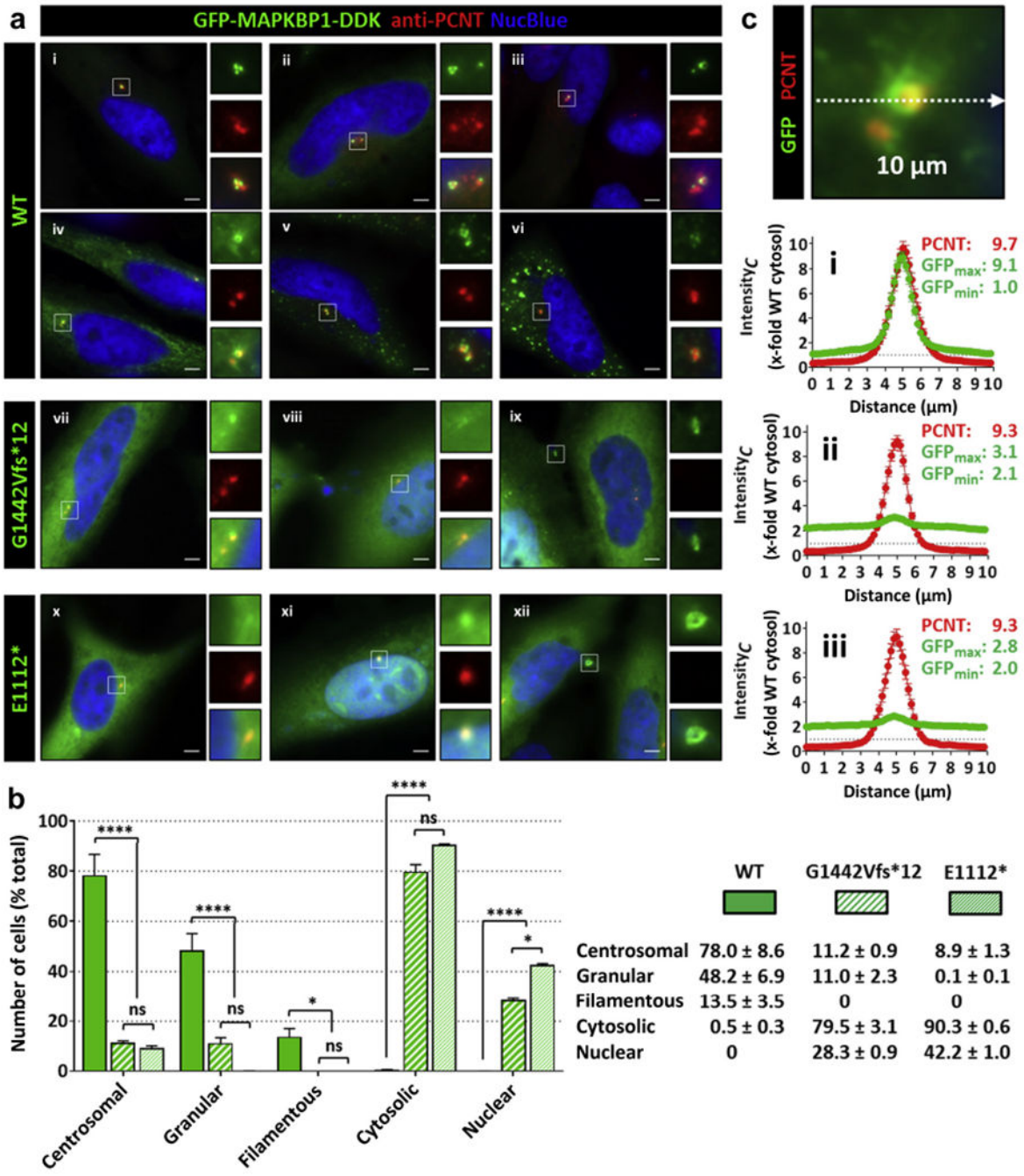

Figure 3 |. C-terminally truncated MAPKBP1 variants show aberrant intracellular localization.

HeLa cells transiently transfected with green fluorescent protein (GFP)/DDK-tagged variants of MAPKBP1 (wild-type [WT] and patient variants G1442Vfs*12 and E1112*) (green) were fixed, permeabilized, and stained with an anti-PCNT antibody (red) as centrosome marker. (**a**) Fluorescence imaging (original magnification ×40) revealed different localization patterns for MAPKBP1 WT: predominantly centrosomal (*i–iii*), centrosomal and filamentous or granular (*iv* and *v*), or predominantly granular (*vi*). Patient variants showed predominantly cytosolic distribution with or without additional nuclear

localization (*vii* and *x* or *viii* and *xi*, respectively) and only faint colocalization with PCNT (zoom images). Frequently, additional localization to the midbody was observed (*ix* and *xii*). Nuclei were stained with NucBlue. Bars = 10 μm. (**b**) Comparison of distribution patterns of between GFP-MAPKBP1 WT and patient variants (mean ± SEM). *$P < 0.0332$; ****$P < 0.0001$. (**c**) Intensity of GFP-MAPKBP1 variants (green) and PCNT (red) was quantified over a distance of ±5 μm around centrosomes and plotted relative to the cytosolic intensity of MAPKBP1 WT (dotted lines): (*i*) WT; (*ii*) G1442Vfs*12; (*iii*) E1112*. $Intensity_C$, intensity at the centrosome; max, maximum; min, minimum; ns, not significant. To optimize viewing of this image, please see the online version of this article at www.kidney-international.org.

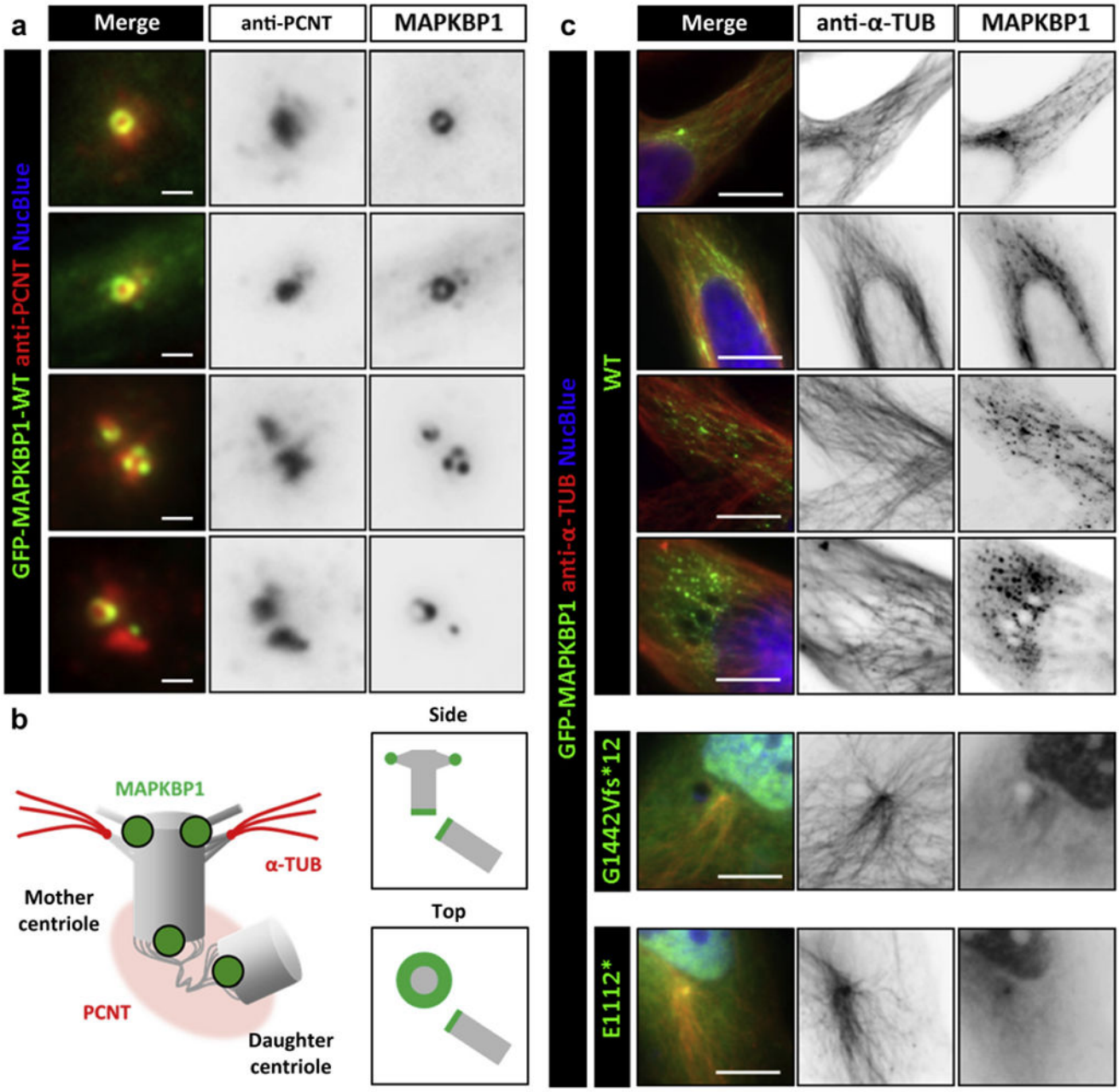

Figure 4 |. Wild-type (WT) MAPKBP1 is associated with centrioles and microtubules.

HeLa cells transiently transfected with green fluorescent protein (GFP)/DDK-tagged variants of MAPKBP1 (WT and patient variants G1442Vfs*12 and E1112*) (green) were fixed, permeabilized, and stained with an (**a**) anti-PCNT (red) or (**c**) anti-α-TUB antibody (red) for fluorescence imaging. (**a**) Detailed imaging of the centrosomes points to a localization of MAPKBP1 WT to the proximal and distal end of the mother and the proximal end of the daughter centriole. Bars = 1 μm. (**b**) Cartoon illustrating potential pattern of MAPKBP1 WT distribution to mother and daughter centrioles. (**c**) MAPKBP1 WT filamentous structures and vesicles colocalize with microtubules, which are reduced for

patient variants. Nuclei were stained with NucBlue. Bars = 10 μm. To optimize viewing of this image, please see the online version of this article at www.kidney-international.org.

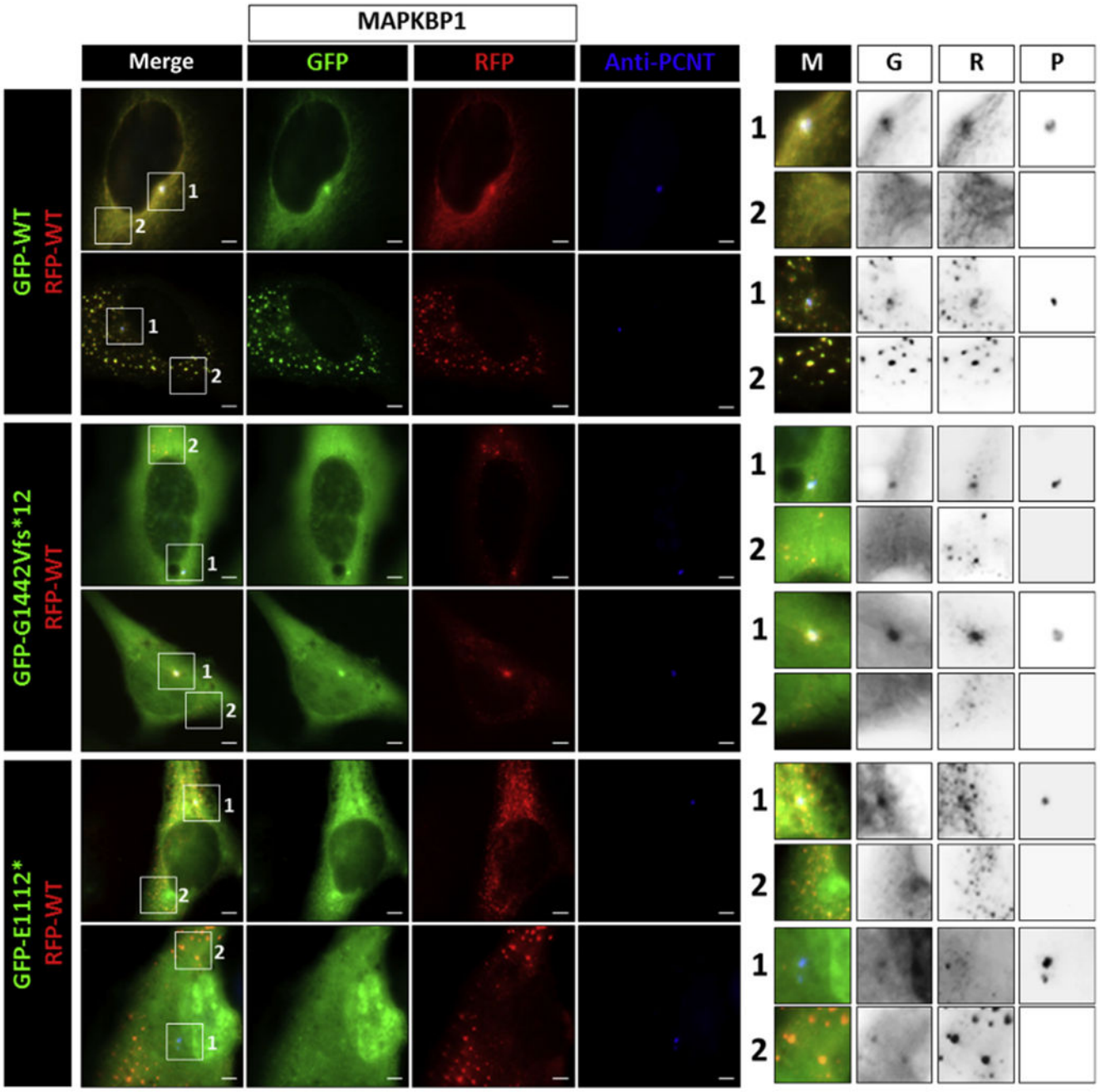

Figure 5 |. Cytosolic and nuclear localization of truncated MAPKBP1 variants is independent of wild-type (WT) expression.

HeLa cells transiently cotransfected with red fluorescent protein (RFP)/DDK-tagged MAPKBP1 WT (R; red) and green fluorescent protein (GFP)/DDK-tagged variants of MAPKBP1 (WT and patient variants G1442Vfs*12 and E1112*) (G; green) were fixed, permeabilized, and stained with an anti-PCNT antibody (P; blue). Fluorescence imaging revealed strong colocalization for differently tagged MAPKBP1 WT proteins, whereas patient variants colocalized at the centrosome in different intensities and rarely to vesicles with low amounts (merge images; M). Nuclei were stained with NucBlue. Bars = 10 μm. To

optimize viewing of this image, please see the online version of this article at www.kidney-international.org.

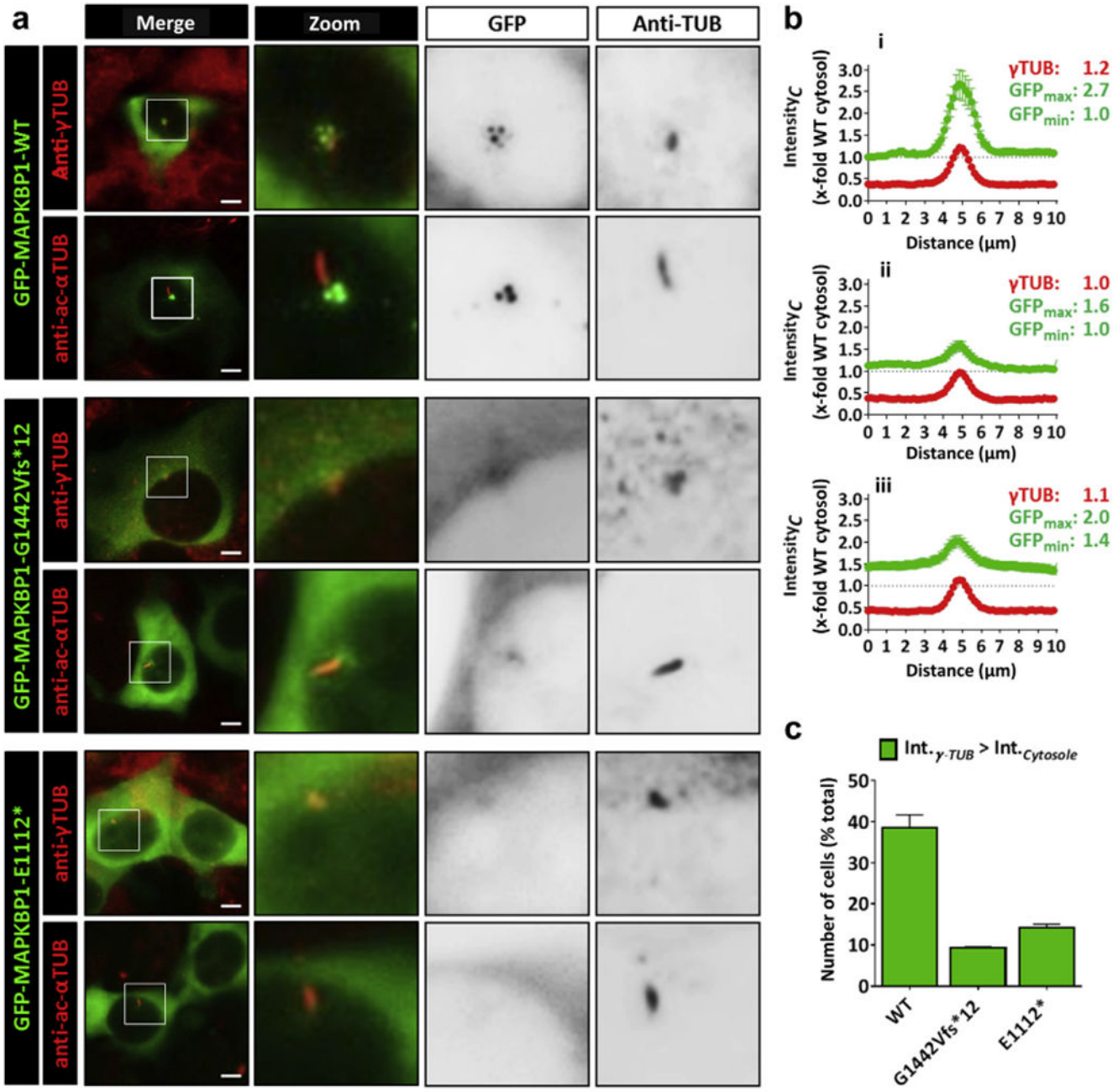

Figure 6 |. Coiled-coil domain allows localization of MAPKBP1 to the basal body of primary cilia.

(**a**) IMCD cells transiently transfected with green fluorescent protein (GFP)/DDK-tagged variants of MAPKBP1 (wild-type [WT] and patient variants G1442Vfs*12 and E1112*) (green) were fixed, permeabilized, and stained with anti-γ-TUB or anti-acetylated-α-TUB (anti-ac-αTUB) antibodies (red) as centrosomal or ciliary marker, respectively. Fluorescence imaging (original magnification ×40) revealed localization of MAPKBP1 WT at the centrosome, ciliary base, and granules, which was reduced or absent in patient variants. Bars = 10 μm. (**b**) Intensity of GFP-MAPKBP1 variants (green) and γ-TUB (red) was quantified

over a distance of ±5 μm around centrosomes and plotted relative to the cytosolic intensity of MAPKBP1 WT (dotted lines): (*i*) WT; (*ii*) G1442Vfs*12; (*iii*) E1112*. (**c**) Quantification of cells with centrosomal GFP intensity (Int) (γ-TUB) exceeding the cytosolic expression level (WT: 38.5 ± 3.1; G1442Vfs*12: 9.3 ± 0.3; E1112*: 14.2 ± 0.9 [number of cells {%}; mean ± SEM]). $Intensity_C$, intensity at the centrosome; max, maximum; min, minimum. To optimize viewing of this image, please see the online version of this article at www.kidney-international.org.

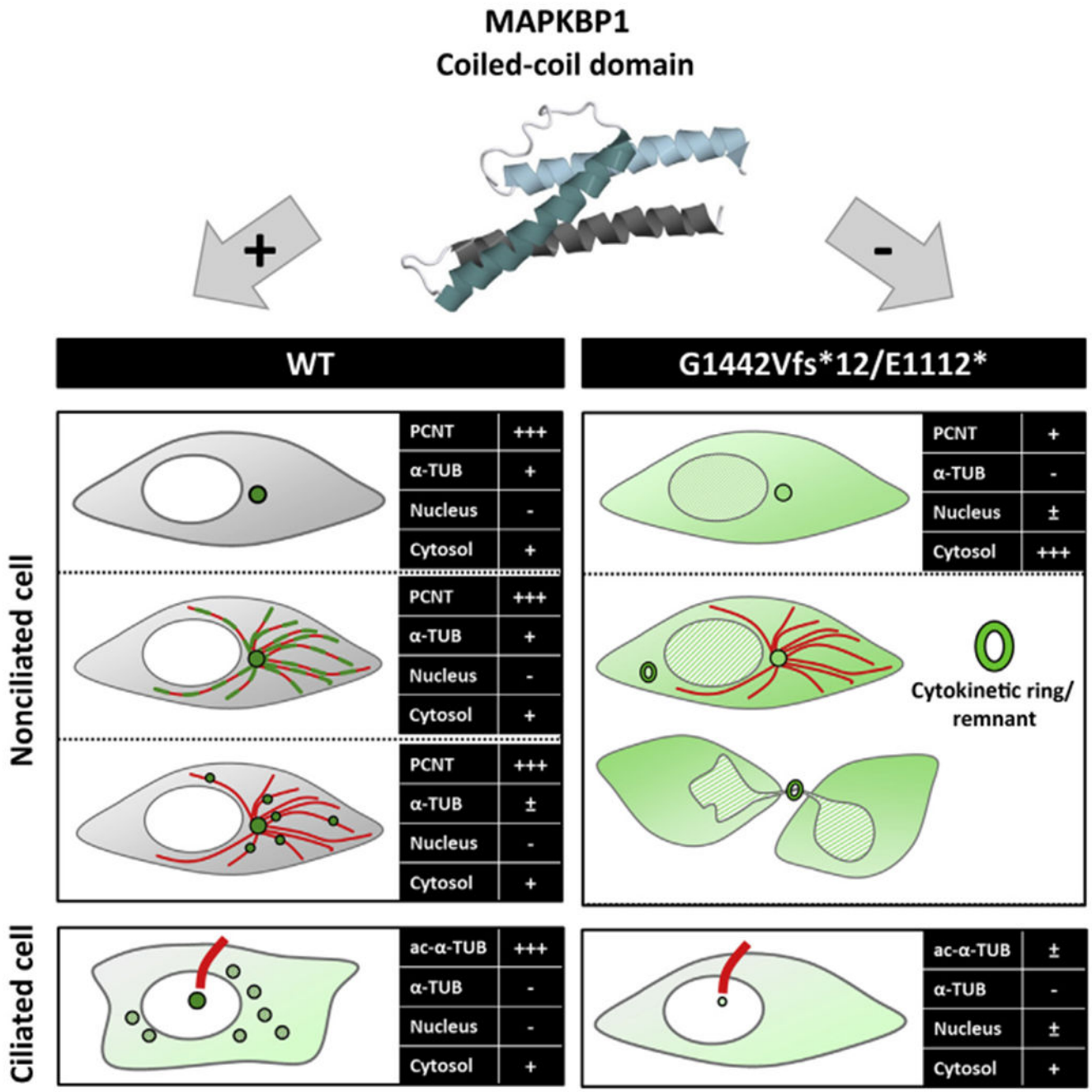

Figure 7 |. MAPKBP1 intracellular localization depending on its coiled-coil domain.

In nonciliated cells, the C-terminal coiled-coil domain of MAPKBP1 wild type (WT) allows efficient centrosomal and microtubule association and is required for the formation of MAPKBP1 granules. C-terminally truncated variants show weaker staining at the centrosome, are predominantly dispersed through the cytosol, and enter the nucleus. A proportion of dividing cells demonstrated intense accumulation of patient variants at the midbody of (aberrantly) dividing cells or its remnant. In ciliated cells, MAPKBP1 WT

mainly localizes to the base of primary cilia and granular structures in contrast to C-terminally truncated patient variants. ac, acetylated.

Table 1 |

Novel pathogenic nephronophthisis-associated *MAPKBP1* variants

Patient	Age, yr	Nucleotide exchange (zygosity)	Protein change	gnomAD/ACMG	PC	Renal function	Kidney morphology	Extrarenal manifestations
1	37	c.4317+5G>C (hom)	p.Gly1442Valfs*12	Not present/ pathogenic	Yes	CKD G5 at age 23 yr; KTx at age 23 yr	Increased echogenicity; solitary cysts (left and right kidney)	Facial dysmorphism with dental overcrowding; scoliosis; ED-like syndrome; mild exophthalmos
2	14	c.3333-2A>G (hom)	p.Arg1111Serfs*5 p.Glu1112Tyrfs*41 p.Pro1113Glufs*2	Not present/ pathogenic	No	CKD G3b at age 14 yr; polyuria; polydipsia	Increased echogenicity; solitary cysts (left and right kidney)	Vascular anomaly: left IVC, growth retardation

ACMG, American College of Medical Genetics and Genomics; CKD, chronic kidney disease; ED, Ehlers-Danlos; G3b, grade 3b; G5, grade 5; gnomAD, Genome Aggregation Database; hom, homozygous; IVC, inferior vena cava; KTx, kidney transplant; PC, parental consanguinity.

Nucleotide and protein nomenclature according to NM_001128608.2 (Online Mendelian Inheritance in Man database).